ACS Partner Journal

CHEMICAL & BIOMEDICAL IMAGING

pubs.acs.org/ChemBioImaging

Article

Probing Oxidant Effects on Superoxide Dismutase 1 Oligomeric States in Live Cells Using Single-Molecule Fluorescence Anisotropy

Huanhuan Chen and Tai-Yen Chen*

Cite This: *Chem. Biomed. Imaging* 2023, 1, 49−57

Read Online

ACCESS | Metrics & More | Article Recommendations | Supporting Information

ABSTRACT: The protein Cu/Zn superoxide dismutase (SOD1) is known to function as a dimer, but its concentration in cells (~50 μM) and the dimerization constant (K_d of 500 μM) results suggest that it exists in a monomer-dimer equilibrium. It is unclear how the oligomeric state of SOD1 changes when cells are initially exposed to high levels of extracellular oxidative stress. To address this problem, we introduced the single-molecule fluorescence anisotropy (smFA) assay to explore SOD1 oligomeric states in live COS7 cells. smFA specifically probes the fluorescence polarization changes caused by molecular rotations where the fast-rotating molecules (either due to smaller hydrodynamic volume or less viscous environments) deteriorate the emission polarization and thus lower the anisotropy. After validating that smFA is effective in distinguishing monomeric and dimeric fluorescence proteins, we overexpressed SOD1 in live COS7 cells and investigated how its oligomeric state changes under basal, 2 h, and 24 h 100 μM H_2O_2 treatments. We found that treating cells with H_2O_2 promotes SOD1 dimerization and decreases cellular viscosity in 2 h. Interestingly, prolonged H_2O_2 treatments show similar results as the basal conditions, indicating that cells return to a steady state similar to the basal state after 24 h, despite the presence of H_2O_2. Our results demonstrate that SOD1 changes its oligomeric state equilibrium in response to extracellular oxidative stresses. smFA will open new opportunities to explore the relationship between the SOD1 oligomer state and its H_2O_2-based signaling and transcription regulation roles.

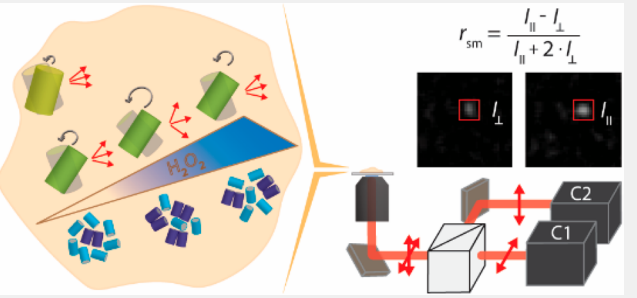

KEYWORDS: *single-molecule fluorescence anisotropy, protein rotation, hydrogen peroxide, H_2O_2, superoxide dismutase 1, SOD1, protein oligomerization, cellular viscosity*

1. INTRODUCTION

Homeostasis of oxidative stress is crucial for normal cellular signaling and functions (e.g., ATP production[1−3] and NADPH oxidase activity[4−7]) but could also be harmful when misregulated. Among multiple antioxidant defense systems,[8−12] Cu/Zn superoxide dismutase (SOD1) is the frontline multifunctional protein that scavenges superoxide radicals, mediates H_2O_2-based metabolism signaling, and regulates antioxidant transcriptions. SOD1 monomers and dimers are both required for antioxidant defense. For example, SOD1 travels through the mitochondrial membrane as a monomer. After entering the mitochondria, its dimerization stabilizes the electrostatic loop to maximize scavenging efficiency. People typically think that SOD1 is mostly dimeric, but based on the concentration of SOD1 in human cell lines (~10−100 μM[13]) and the dimerization constant (K_d of 100 μM to 1 mM[13−15]), a simple dimerization model would predict that SOD1 is 80% monomeric and 20% dimeric. Such observations suggest that there are active processes that must be oxidative stress-sensitive to control dimerization dynamics. Unfortunately, most studies investigating SOD1 oligomerization were done in vitro[16,17] and thus ignored the effects of the native cellular environment and interacting partners, leaving the physiological significance of studies unclear. It is still challenging to address this hypothesis because of the lack of tools to probe SOD1 oligomerization in cells.

Steady-state fluorescence anisotropy (FA),[18−23] a technique monitoring the difference between parallelly and perpendicularly polarized emission intensities under excitation with polarized light, has been widely utilized in probing proteins' oligomeric states. The basic principle of detecting oligomeric state is based on fluorescence depolarization due to Förster Resonance Energy Transfer between the same type of fluorophores (homo-FRET, fluorophore serves as donor and acceptor) or molecular rotation. Unlike the typical FRET process, where the excited donor transfers excited state energy to an acceptor fluorophore with longer emission wavelengths,

Received: January 4, 2023
Revised: February 3, 2023
Accepted: February 8, 2023
Published: March 6, 2023

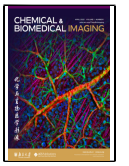

homo-FRET relaxes energy to the same type of fluorophore nearby due to the donor's emission overlaps with its own absorption spectra. The requirement of a single fluorophore makes homo-FRET a promising assay to investigate the protein oligomeric states by nicely addressing the uncontrollable cotransfections of donor and acceptor dyes.

Technically, since the fluorophore acts as both the FRET donor and acceptor in homo-FRET, one needs to estimate the degree of homo-FRET by calculating the FA instead of the typical FRET efficiency. The occurrence of homo-FRET will lead to a decrease in anisotropy, which occurs due to different transition dipole directions of the FRET donor and acceptor pairs. On the other hand, faster molecular rotation also deteriorates the emission polarization and thus lowers anisotropy. However, considering the transition from monomer to dimer, the dimer formation will slow down the rotation (i.e., increase FA) and increase homo-FRET (i.e., decrease FA), antagonistically affecting the FA and limiting its usage. To address this dilemma and maximize the benefit of FA, one should use only the rotation or homo-FRET principle. Using photoswitchable fluorescent protein Dronpa, the Patterson group specifically modulated homo-FRET processes.[24,25] By monitoring real-time FA changes upon photoswitching fluorescent protein off, they successfully differentiated Dronpa tandem oligomers. Despite these exciting results, the ensemble approach does not provide the spatial distribution of oligomers. Considering recent successes in using single-molecule super-resolution microscopy to study various biophysical processes,[26−31] it is tempting to combine this method with other biophysical techniques to investigate protein oligomer behavior in a highly resolved manner across a range of cell types.

Here, we develop a single-molecule fluorescence anisotropy (smFA) assay to investigate the effects of a common oxidant, hydrogen peroxide (H_2O_2), on SOD1 oligomeric states in live COS7 cells. We conducted the single-molecule FA measurement to probe the SOD1 oligomer information using molecular rotation information. By replacing the FRET donor from constant fluorescent to photoconvertible fluorescent proteins mEos4b,[32] we abolished the homo-FRET pathway by switching the mEos4b emission to a longer wavelength and avoiding the spectral overlap with the donor absorption. We generated monomeric mEos4b (mE) and dimeric mEos4b (dmE) controls to validate the smFA assay via the rotation-dependent FA property. Compared to the ensemble FA measurements, we found that smFA results show larger FA differences between mE and dmE, indicating that smFA effectively removes homo-FRET complications. By applying smFA to quantify FA of SOD1 labeled with mEos4b ($SOD1^{mE}$) in cells under basal conditions and comparing the results with the mE controls, we discovered that $SOD1^{mE}$ existed as a mixture of monomers and dimers. Treating cells with H_2O_2 for 2 h will temporarily decrease intracellular viscosity and promote $SOD1^{mE}$ dimerization. But the cells and $SOD1^{mE}$ will return to the steady state again after 24 h treatments. These findings suggest that the smFA assay is sensitive to probe oligomeric state changes of cytosolic proteins. More importantly, our results provide information on $SOD1^{mE}$ oligomeric state changes under basal and H_2O_2 treatments, highlighting that H_2O_2 modulates SOD1 structure to induce cellular antioxidant defense.

2. RESULTS AND DISCUSSION

2.1. Fluorescence Anisotropy at the Single-Molecule or Single-Cell Levels Differentiates Monomers from Dimers in Live Cells

To demonstrate that smFA is effective in distinguishing different oligomers, we generated two control constructs (Methods, section 4.1), monomeric mEos4b (mE, 27 kDa) and dimeric mEos4b (dmE, 53 kDa). mEos4b is a photoconvertible fluorescence protein that is naturally green fluorescent but becomes red fluorescent after photoconversion. Protein gel analysis shows that both mE and dmE are intact (i.e., no cleaved bands observed) in the cells (Figure 1A). All smFA measurements were conducted by transfecting the control constructs in live COS7 cells.

Using a home-built smFA setup with a 3 ms exposure time (Figure 1B, Methods, section 4.2), we tracked the fluorescence intensity of photoconverted mEos4b proteins in cells until they photobleached. The constructs were excited with a parallel-polarized light. Their fluorescence passed the polarization beam splitter and was recorded by the scientific complementary metal oxide semiconductor (CMOS) camera to report the parallel and perpendicular polarized fluorescence micrograph. These fluorescence micrographs were processed by the home-built MATLAB program (Figure 1C) to identify the locations of every single molecule and quantify the parallel and perpendicular polarized fluorescence intensities. In short, the micrographs from the parallel (Im_1) and perpendicular (Im_2) polarized channels were first used to generate composite images (Im_{com}) via $Im_{com} = Im_1 + 2 \times Im_2$ for identifying molecular localizations (Figure 1C). With the identified locations, we further determine fluorescence intensities at the parallel ($I_{\parallel}$) and perpendicular($I_{\perp}$) polarized images to calculate single-molecule fluorescence anisotropy, r_{sm}, using $r_{sm} = \frac{I_{\parallel} - I_{\perp}}{I_{\parallel} + 2 \cdot I_{\perp}}$. Combining r_{sm} of all single-molecule spots, we obtained the probability distribution function of fluorescence anisotropy, PDF(r_{sm}), for target proteins. It is worth noting that all detected single-molecule signals originated from the photoconverted mEos4b (i.e., red emission fluorescence). This experimental setup eliminates the possibility of homo-FRET, making the rotation the only contributor to the smFA changes.

We first examined mE and dmE in live COS7 cells under basal conditions at 25 °C. Figure 2A shows single-molecule fluorescence images from the parallel and perpendicular channels of mE and dmE, respectively. Compared with mE, dmE shows a larger intensity difference between the two channels. The averaged r_{sm} maps (averaging all r_{sm} within each pixel) also indicate dmE has more pixels with larger r_{sm} (Figure 2B). We further select cells with similar expression ranges for subsequent analysis (Figure 2C). Figure 2D and Figure 2E shows the normalized smFA distributions, PDF(r_{sm}), established from all r_{sm} (more than 15×10^5 smFA for each condition) from cells overexpressed mE (29 cells) and dmE (24 cells). Both PDF(r_{sm}) of mE and dmE were sufficiently fitted by Gaussian distributions. Compared to the mE results, the dmE shows a larger smFA peak and a slightly narrower smFA distribution (i.e., narrower full width at half maximum, $fwhm_{dmE} = 0.268 \pm 0.003$ vs $fwhm_{mE} = 0.278 \pm 0.003$). To ensure our reported smFA values are statistically saturated and robustly reveal the FA, we further examined how the averaged single-molecule fluorescence anisotropy ($\overline{r_{sm}}$) changes with the number of r_{sm}. Figure 2F shows that fluctuations of the $\overline{r_{sm}}$

https://doi.org/10.1021/cbmi.3c00002
Chem. Biomed. Imaging 2023, 1, 49−57

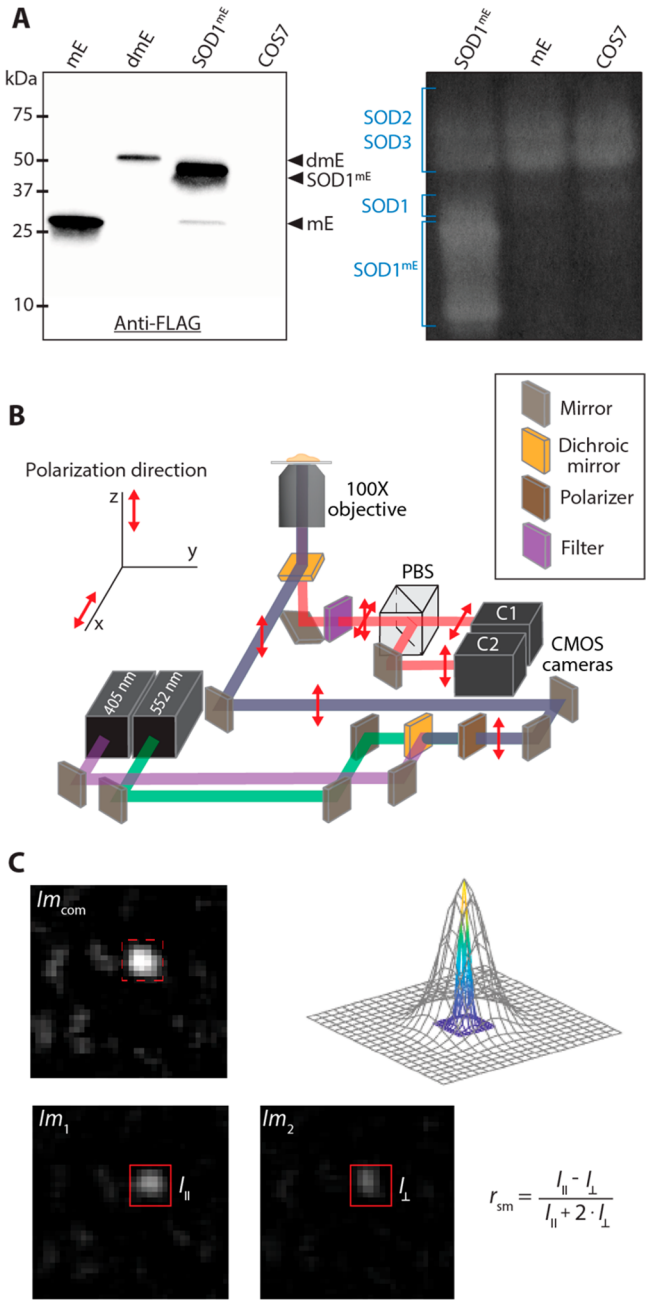

Figure 1. Sample characterizations and single-molecule polarization microscope setup. (A) Western blot results (left) and antioxidant activity assay (right) of mE, dmE, and SOD1^{mE}. Expressed dmE are intact, while SOD1^{mE} has ~5% cleavage. SOD1^{mE} maintains antioxidant functions. (B) Experimental setup for smFA measurements. Coaxially aligned activation (405 nm laser, purple) and excitation (552 nm laser, green) lasers passed through the polarizer to linearly excite the photoconverted mE (red double-headed arrow). Emission from photoconverted mE was collected by the objective, separated into parallelly and perpendicularly polarized components by a polarization beam splitter (PBS), and recorded by a CMOS camera. (C) Scheme for smFA calculation. Im_{com} data were fit with a two-dimensional Gaussian function to localize the single-molecule signals. Corresponding intensity in Im_1 and Im_2 were extracted out to calculate smFA, r_{sm}.

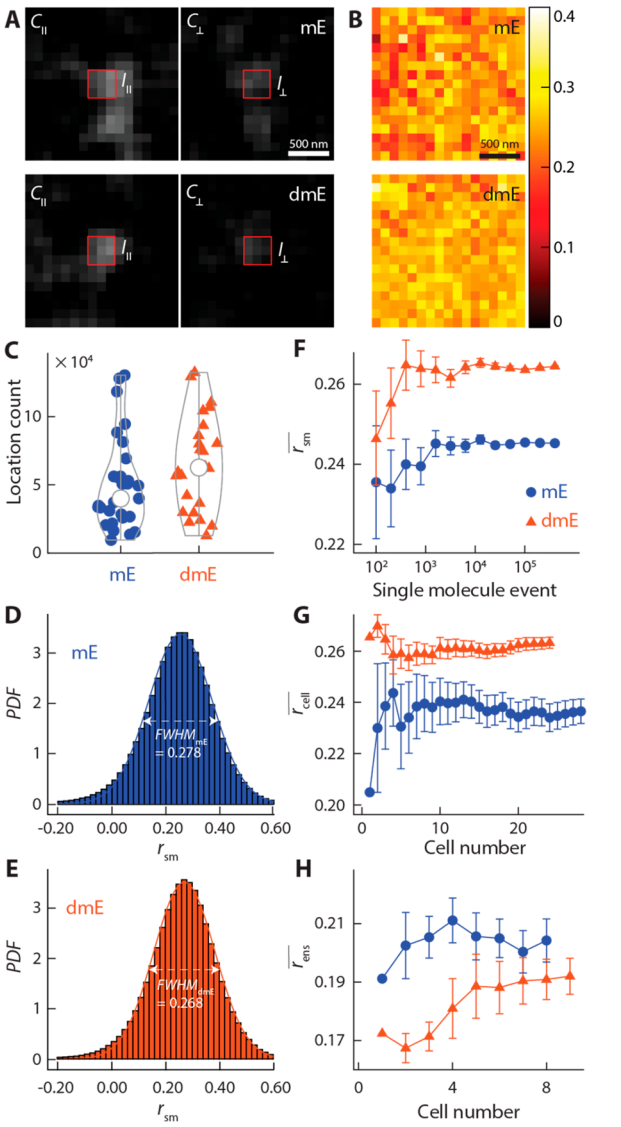

Figure 2. Fluorescence anisotropy results of mE and dmE controls at the single-molecule, single-cell, and ensemble levels. (A) Single-molecule image from the parallel and perpendicular channels of mE and dmE, respectively. (B) Averaged r_{sm} maps of mE and dmE. Overall dmE has more pixels with larger averaged r_{sm} compared with mE. (C) Cellular protein concentrations of cells overexpressed mE or dmE. mE and dmE samples have similar expression levels. (D,E) PDF(r_{sm}) of mE (D) and dmE (E). mE gives a larger peak width (fwhm) compared with dmE. (F−H) Averaged fluorescence anisotropy plots of mE and dmE at the single-molecule (F, $\overline{r_{sm}}$), single-cell (G, $\overline{r_{cell}}$), and ensemble level (H, $\overline{r_{ens}}$). Both $\overline{r_{sm}}$ and $\overline{r_{cell}}$ results clearly show that dmE has a larger fluorescence anisotropy than mE ($\overline{r_{sm}^{dmE}}$ = 0.2640 ± 0.0002, $\overline{r_{sm}^{mE}}$ = 0.2450 ± 0.0002; $\overline{r_{cell}^{dmE}}$ = 0.263 ± 0.002, $\overline{r_{cell}^{mE}}$ = 0.237 ± 0.005). In contrast, $\overline{r_{ens}}$, due to the effects of homo-FRET, dmE has a smaller FA compared with mE ($\overline{r_{ens}^{dmE}}$ = 0.192 ± 0.006, $\overline{r_{ens}^{mE}}$ = 0.204 ± 0.007). All errors were estimated using standard error of the mean (SEM).

decrease with an increasing number of r_{sm}. The $\overline{r_{sm}}$ stabilizes ($\overline{r_{sm}^{mE}}$ = 0.2450 ± 0.0002 vs $\overline{r_{sm}^{dmE}}$ = 0.2640 ± 0.0002) once the number of r_{sm} is greater than 30000, indicating the reported values are indeed statistically saturated.

The physical parameters that affect FA are typically described by the Perrins equation[33,34]

https://doi.org/10.1021/cbmi.3c00002
Chem. Biomed. Imaging 2023, 1, 49−57

$$r = \frac{r_0}{1 + \tau_{Fl} kT/\eta(T)V} \quad (1)$$

where the r is the measured fluorescence anisotropy, r_0 is the inherent fluorescence anisotropy (limiting anisotropy ~0.4) for a static distribution of fluorophores, and τ_{Fl} is the measured fluorescence lifetime. T is the temperature, $\eta(T)$ is the temperature-dependent viscosity of the medium, V is the hydrodynamic molecular volume, and k is the Boltzmann constant. Considering experiments were performed using the same fluorophore (photoconverted mEos4b) and cell system (COS7 cells) under constant temperature (25 °C), we conclude the τ_{Fl}, η(T), and T were constants for both mE and dmE conditions. In other words, the change of fluorescence anisotropy r is mainly contributed by the changes in hydrodynamic molecular volume V. Indeed, compared to the mE, the 53 kDa dmE has a larger hydrodynamic volume, which would be more sensitive to surrounding environmental viscosity and results in a slow and restricted rotation and, thus, a larger FA.

To compare our results to the ensemble FA measurements, we also conducted similar analyses at the single-cell levels. Specifically, the fluorescence anisotropy of each cell (r_{cell}) was calculated by averaging all r_{sm} detected within the cell. We combined r_{cell} over more than 20 cells to estimate the final averaged cellular fluorescence anisotropy ($\overline{r_{cell}}$). Figure 2G demonstrates that $\overline{r_{cell}}$ values stabilize ($\overline{r_{cell}^{mE}} = 0.237 \pm 0.005$ and $\overline{r_{cell}^{dmE}} = 0.263 \pm 0.002$) after averaging over 10 cells. Like r_{sm} results, r_{cell} results also clearly reveal that the dmE has higher fluorescence anisotropy than the mE.

In contrast, the ensemble fluorescence anisotropy ($\overline{r_{ens}}$) measurements using mEos4b green fluorescence (Methods, section 4.3) gave unexpected results (Figure 2H), where the dmE shows a smaller $\overline{r_{ens}}$ than the mE ($\overline{r_{ens}^{dmE}} = 0.192 \pm 0.006$, $\overline{r_{ens}^{mE}} = 0.204 \pm 0.007$). Another noticeable difference is that ensemble fluorescence anisotropy measurements show smaller FA values. The observed small $\overline{r_{ens}}$ differences may not be surprising since it probes the collective effects of homo-FRET and molecular rotations. For transitions from mE to dmE, one would expect to observe the effects of slower molecule rotations and homo-FRET. There is no doubt that the increase in protein size leads to slower molecule rotations or larger hydrodynamic volume and, thus, larger $\overline{r_{ens}}$. However, homo-FRET results in the excitation of neighbor emitters with different polarization, giving a decreased $\overline{r_{ens}}$. These two processes cancel each other and minimize the $\overline{r_{ens}}$ differences between mE and dmE.

Compared to the $\overline{r_{ens}}$, our results suggest that using FA at the single-molecule ($\overline{r_{sm}}$) or single-cell ($\overline{r_{cell}}$) could robustly report larger FA differences between mE and dmE. This is because our approach eliminates the effects of homo-FRET and specifically detects the effects of molecule rotations. We thus conclude that fluorescence anisotropy at the single-molecule or single-cell levels differentiates monomers from dimers in live cells.

2.2. Single-Molecule Fluorescence Anisotropy of mEos4b Reveals the Effects of H_2O_2 on Intracellular Viscosity

The comparison between mE and dmE under basal conditions, where fluorescence lifetime (τ_{Fl}), intracellular viscosity (η), and temperature (T) are constants while hydrodynamic volume (V) is the only variable, demonstrates that smFA is effective in distinguishing different protein oligomers. However, the interpretation of smFA gets more challenging when investigating the effects of H_2O_2 on protein oligomers under constant T. This complication originates from the fact that H_2O_2 may modulate τ_{Fl} of photoconverted mE, the η, or the V. To understand the effects of H_2O_2 on the SOD1 oligomeric state changes, one first needs to dissect the effects of H_2O_2 on the τ_{Fl} and η.

To address this complication, we performed smFA measurements using cells overexpressed mE under basal and H_2O_2 treatments at 25 °C. Typically, cellular responses to H_2O_2 by modulating the production of antioxidant enzymes, heat shock response, and mitochondrial enzyme activation. These processes occur within hours of exposure, and the cells eventually reach a new steady state. To catch these changes and understand the response of SOD1 toward H_2O_2, we further examined SOD1 oligomeric states when cells are under 2 h (i.e., during responses) and 24 h (i.e., re-establish a new steady state) H_2O_2 treatments. Since the mE only presents in the monomeric form and is not affected by H_2O_2 treatments (Figure S1), it provides a nice platform to abolish the contribution of V to the r_{sm}. By quantifying the r_{sm} of mE at a constant temperature (Methods, section 4.2), we can distill how the H_2O_2 treatment influences τ_{Fl} and η.

Figure 3A–C shows PDF(r_{sm}) of cells overexpressed mE under basal (29 cells) and 100 μM H_2O_2 for 2 h (17 cells) and 24 h (9 cells) conditions. Each PDF(r_{sm}) was generated using more than 4×10^5 smFA and fitted with a Gaussian function. The single-molecule event-dependent $\overline{r_{sm}}$ plot (Figure 3D) again shows the stabilized and statistically saturated $\overline{r_{sm}}$ for all conditions: $\overline{r_{sm,basal}^{mE}} = 0.2450 \pm 0.0002$, $\overline{r_{sm,2h}^{mE}} = 0.2310 \pm 0.0002$, and $\overline{r_{sm,24h}^{mE}} = 0.2420 \pm 0.0003$. When switching from basal to oxidatively stressed conditions, the $\overline{r_{sm}^{mE}}$ significantly decreases in 2 h and gradually recovers to similar basal conditions after 24 h. A similar trend was also observed in the fwhm of the PDF(r_{sm}^{mE}), where the 2 h H_2O_2 treatment gives the largest width ($fwhm_{sm,2h}^{mE} = 0.313 \pm 0.003$) compared to the other two conditions ($fwhm_{sm,basal}^{mE} = 0.278 \pm 0.003$ and $fwhm_{sm,24h}^{mE} = 0.261 \pm 0.002$).

Based on the Perrins equation (eq 1), the decreased $\overline{r_{sm}^{mE}}$ of cells under 2 h H_2O_2 treatments can be explained by longer τ_{Fl} or the lower η. However, recent fluorescence lifetime imaging of membrane-anchored dye BODIPY1 reports that the dye lifetime actually decreases linearly over time under H_2O_2 treatments.[35] If the τ_{Fl} indeed dictates the $\overline{r_{sm}^{mE}}$, one should expect an increased, instead of decreased, $\overline{r_{sm}^{mE}}$. We thus conclude that the τ_{Fl} can not be the main reason for these experimental observations.

This analysis indicates the observed $\overline{r_{sm}^{mE}}$ change must be related to the shift in η. By rearranging eq 1, we can obtain

$$\frac{1}{r} = \left(\frac{b}{\eta} + 1\right) \cdot c \quad (2)$$

where $b = \frac{\tau_{Fl} kT}{V}$ and $c = \frac{1}{r_0}$ are constants for the current experimental setup. It is clear that lower cellular viscosity will lead to smaller fluorescence anisotropy. It is likely that changes in protein concentrations could either positively or negatively

https://doi.org/10.1021/cbmi.3c00002
Chem. Biomed. Imaging 2023, 1, 49–57

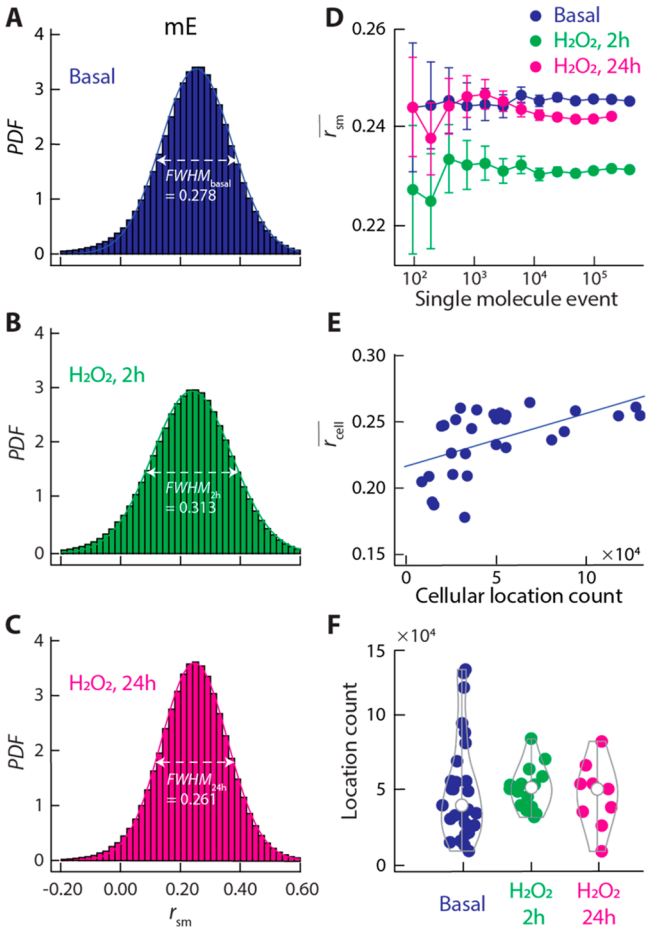

Figure 3. Fluorescence anisotropy result of mE under basal and H_2O_2 stressed conditions. (A–C) PDF(r_{sm}) of mE under the basal condition (A), 2 h (B), or 24 h (C) 100 μM of H_2O_2 treatments. The 2 h H_2O_2 treatment gives the largest fwhm while basal and 24 h H_2O_2 treatment give similar fwhm. (D) Averaged fluorescence anisotropy ($\overline{r_{sm}}$) plot of mE. Cells under 2 h H_2O_2 treatment give the smallest $\overline{r_{sm}}$ while basal and 24 h H_2O_2 treatment present similar fluorescence anisotropy ($\overline{r^{mE}_{sm,basal}}$ = 0.2450 ± 0.0002, $\overline{r^{mE}_{sm,2h}}$ = 0.2310 ± 0.0002, and $\overline{r^{mE}_{sm,24h}}$ = 0.2420 ± 0.0003). (E) Cellular fluorescence anisotropy versus single-molecule locations (an analogue of protein concentration) plot of mE under basal condition ($r^{mE}_{cell,basal}$). $r^{mE}_{cell,basal}$ increase linearly with higher protein concentrations. (F) Relative cellular mE concentrations under 3 conditions estimated from single-molecule locations. Most cells with 2 h H_2O_2 treatment are highly expressed (location count >3 × 10^4), while the other two conditions have broader protein concentration distribution. All errors were estimated using SEM.

impact intracellular crowdedness and change intracellular matrix stiffness. Indeed, we did observe $\overline{r^{mE}_{cell}}$ decreases linearly with lower protein concentration when we conducted the fluorescence anisotropy analysis at the single-cell levels (Figure 3E). The decrease in $\overline{r^{mE}_{sm}}$ will suggest a reduction in intracellular mE abundance. However, by using the detected single-molecule events as an indication of intracellular protein concentration, Figure 3F shows that cells with the 2 h H_2O_2 treatment have the highest averaged protein concentration among the three conditions, which can not explain the decreased $\overline{r^{mE}_{sm}}$. These data collectively imply that the change in η is not related to the intracellular mE abundance. Since the reduction in η can't be explained by the change of mE abundance, the possible explanation would be the H_2O_2 treatment somehow decreases intracellular viscosity, which in turn lowers the η.

2.3. Single-Molecule Fluorescence Anisotropy of SOD1-mEos4b Reveals That H_2O_2 Promotes SOD1 Dimerization in Cells

After examining how H_2O_2 affects non-oligomer-related properties, we applied this methodology to probe how cells may modulate the oligomeric state of the cytosolic SOD1 upon H_2O_2 treatments. The functional and intact SOD1-mEos4b ($SOD1^{mE}$) construct was overexpressed in COS7 cells (Figure 1A). Cells under basal conditions or treated with 100 μM H_2O_2 for 2 or 24 h were imaged at 25 °C. The complication of protein concentrations was reduced by selecting cells with similar $SOD1^{mE}$ levels for subsequent analysis and comparisons.

Figure4A shows the single-molecule fluorescence images from parallel and perpendicular channels for cells under basal,

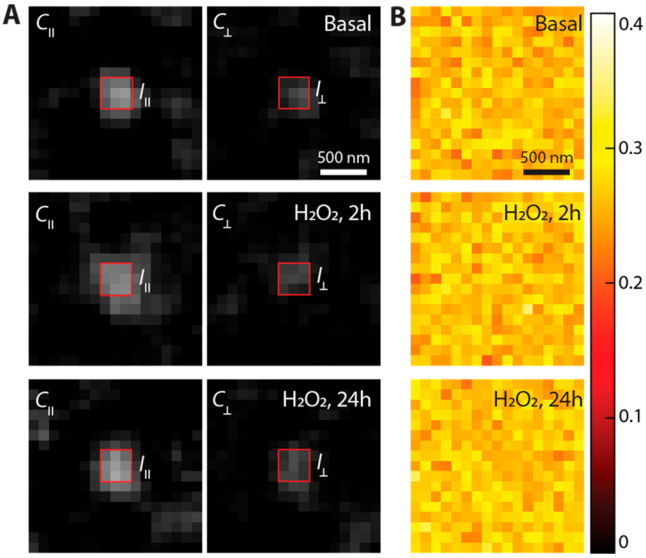

Figure 4. Fluorescence anisotropy images of $SOD1^{mE}$ under various conditions. (A) Single-molecule image from the parallel and perpendicular channels of basal, 2 h H_2O_2, and 24 h H_2O_2 treatments. (B) r_{sm} maps show similar results for all conditions.

2 h H_2O_2, and 24 h H_2O_2 treatments. All conditions show similar intensities. r_{sm} maps were also calculated for each condition (Figure 4B), where no distinguishable difference was observed. Figure 5A–C shows PDF(r_{sm}) of cells overexpressed $SOD1^{mE}$ under basal (26 cells) and 100 μM H_2O_2 for 2 h (20 cells) and 24 h (7 cells) conditions. Each PDF(r_{sm}) was generated using more than 5 × 10^5 smFA to ensure data saturation and fitted with a Gaussian function. The single-molecule event-dependent $\overline{r_{sm}}$ plot (Figure 5D) reports the $\overline{r^{SOD1^{mE}}_{sm}}$ for all conditions: ($\overline{r^{SOD1^{mE}}_{sm,basal}}$ = 0.2630 ± 0.0001, $\overline{r^{SOD1^{mE}}_{sm,2h}}$ = 0.2620 ± 0.0002, and $\overline{r^{SOD1^{mE}}_{sm,24h}}$ = 0.2640 ± 0.0003). Interestingly, we did not observe significant $\overline{r^{SOD1^{mE}}_{sm}}$ changes when switching from basal to oxidatively stressed conditions, regardless of the H_2O_2 treatment durations. However, the fwhm of the PDF($r^{SOD1^{mE}}_{sm}$) of the 2 h H_2O_2 treatment gives the largest width, while the other two conditions show the same

https://doi.org/10.1021/cbmi.3c00002
Chem. Biomed. Imaging 2023, 1, 49–57

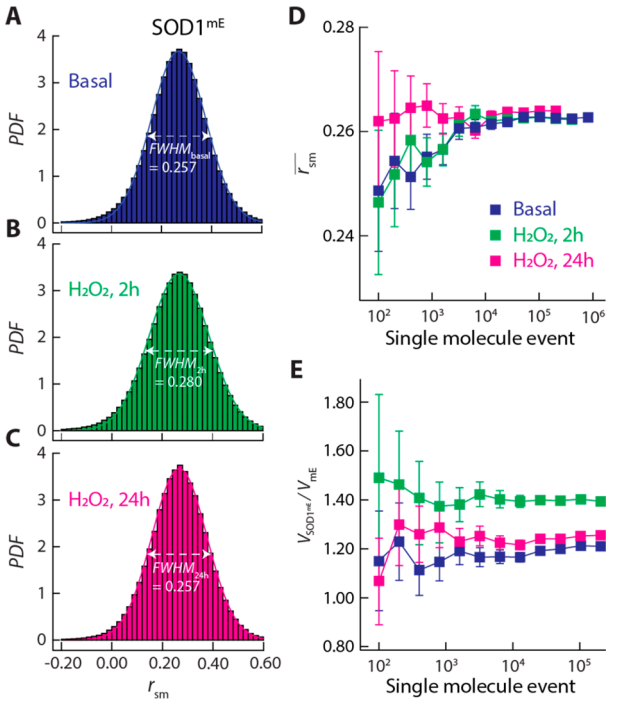

Figure 5. Fluorescence anisotropy result of SOD1^{mE} under basal and H_2O_2 stressed conditions. (A–C) PDF(r_{sm}) of SOD1^{mE} under the basal condition (A), 2 h (B), or 24 h (C) 100 μM of H_2O_2 treatments. The 2 h H_2O_2 treatment gives the largest fwhm, while the basal and 24 h H_2O_2 treatments give the same values. (D) Averaged fluorescence anisotropy ($\overline{r_{sm}}$) plot of SOD1^{mE} under different conditions. All three conditions give similar results ($\overline{r}^{SOD1^{mE}}_{sm,basal}$ = 0.2630 ± 0.0001, $\overline{r}^{SOD1^{mE}}_{sm,2h}$ = 0.2620 ± 0.0002, and $\overline{r}^{SOD1^{mE}}_{sm,24h}$ = 0.2640 ± 0.0003). (E) Relative hydrodynamic volume $\left(\frac{V_{SOD1^{mE}}}{V_{mE}}\right)$ under three conditions. Cells with H_2O_2 treatments both have larger relative hydrodynamic volumes compared to the ones under basal conditions ($\frac{V^{SOD1^{mE}}_{basal}}{V^{mE}_{basal}}$ = 1.212 ± 0.005, $\frac{V^{SOD1^{mE}}_{2h}}{V^{mE}_{2h}}$ = 1.389 ± 0.006, $\frac{V^{SOD1^{mE}}_{24h}}{V^{mE}_{24h}}$ = 1.262 ± 0.005). Also, 2 h H_2O_2 treatment gives the largest relative hydrodynamic value. Errors in D were estimated using SEM. Errors in E were calculated via error propagation.

values (fwhm$^{SOD1^{mE}}_{sm,basal}$ = 0.257 ± 0.003, fwhm$^{SOD1^{mE}}_{sm,2h}$ = 0.280 ± 0.002, fwhm$^{SOD1^{mE}}_{sm,24h}$ = 0.257 ± 0.002). The same H_2O_2-induced fwhm$_{sm}$ changes between the mE and SOD1^{mE} experiments suggest fwhm is more sensitive to the changes in intracellular viscosity than the $\overline{r_{sm}}$.

Since the experiments were conducted at a constant temperature and the fluorescence lifetime does not affect the fluorescence anisotropy, the detected r_{sm} here reports the overall effects of intracellular viscosity and the oligomeric state changing under oxidative stress. To understand the effects of H_2O_2 on SOD1^{mE} oligomeric state, we derived $\frac{V_{SOD1^{mE}}}{V_{mE}}$ to exclude viscosity contribution and examined changes in $\frac{V_{SOD1^{mE}}}{V_{mE}}$ under basal and H_2O_2 treatments. By rearranging eq 1, one can express the viscosity of mE and SOD1^{mE} as eqs 3 and 4, respectively.

$$\frac{1}{\eta} = \frac{V_{mE}}{\tau_{FI} kT} \cdot \left(\frac{r_0}{\overline{r_{mE}}} - 1 \right) \tag{3}$$

$$\frac{1}{\eta} = \frac{V_{SOD1^{mE}}}{\tau_{FI} kT} \cdot \left(\frac{r_0}{\overline{r_{SOD1^{mE}}}} - 1 \right) \tag{4}$$

Since the intracellular viscosity is a cell property and is not affected by mE or SOD1^{mE}, eq 3 and eq 4 are thus equivalent. We can thus remove the η in eq 3 by substituting $1/\eta$ with eq 4, which gives the relationship between V_{mE} and $V_{SOD1^{mE}}$ as

$$\frac{V_{SOD1^{mE}}}{V_{mE}} = \frac{\frac{1}{\overline{r_{mE}}} - \frac{1}{r_0}}{\frac{1}{\overline{r_{SOD1^{mE}}}} - \frac{1}{r_0}} \tag{5}$$

Considering V_{mE} is a constant, $\frac{V_{SOD1^{mE}}}{V_{mE}}$ can be interpreted as an analogue of SOD1^{mE} oligomeric states under different conditions.

Figure 5E shows the $\frac{V_{SOD1^{mE}}}{V_{mE}}$ calculated from the $\overline{r_{sm}}$ data of mE (Figure 3D) and SOD1^{mE} (Figure 5D) for cells under basal and oxidative stressed conditions. The $\frac{V_{SOD1^{mE}}}{V_{mE}}$ reaches a maximum after 2 h, indicating that SOD1^{mE} dimerizes after H_2O_2 treatments. Prolonged H_2O_2 treatments result in a similar $\frac{V_{SOD1^{mE}}}{V_{mE}}$, indicating cells adapt to the highly oxidative environments and the SOD1 re-establish a new monomer-dimer equilibrium 24 h.

The intracellular concentration of H_2O_2, a common oxidizing agent and a key cellular signaling molecule, is tightly regulated to minimize its potential to cause cellular damage.[36] However, how cells respond to excess H_2O_2 and modulate the properties of the frontline antioxidant protein, SOD1, in live cells remains unclear due to the lack of proper methodology. By developing single-molecule fluorescence anisotropy (smFA) assay and comparing single-molecule fluorescence anisotropies (r_{sm}) of mE, dmE, and SOD1^{mE} in live COS7 cells under basal and H_2O_2 treatments at a constant temperature, we reported here that H_2O_2 modulates intracellular matrix viscosity and SOD1 oligomeric states when cells under oxidative stresses.

The smFA assay was first validated using mE and dmE under basal conditions. The larger $\overline{r_{sm}}$ of dmE than mE ($\overline{r}^{mE}_{sm}$ = 0.2450 ± 0.0002 vs $\overline{r}^{dmE}_{sm}$ = 0.2640 ± 0.0002) indicates that our smFA assay is capable of distinguishing the molecular rotational difference between proteins with different oligomeric sizes. Considering (i) the $\overline{r_{sm}}$ originated from the combined effect of viscosity of the environment (i.e., intracellular matrix) and hydrodynamic volume of fluorophore and (ii) the hydrodynamic volume of mE remains a constant regardless of the presence of H_2O_2 treatment, we investigated the effects of H_2O_2 on intracellular matrix viscosity by comparing the $\overline{r_{sm}}$ of mE under basal and H_2O_2 treatments with 2 and 24 h. When switching from basal to H_2O_2 treatments, the $\overline{r_{sm}}$ of mE decreases, reaches the lowest value at 2 h, and recovers to a similar value of basal level at 24 h, indicating H_2O_2 affects intracellular viscosity temporarily. Lastly, the same experiments were conducted to examine the effect of H_2O_2 on SOD1 oligomeric states. To specifically study the oligomeric state, we derived $V_{SOD1^{mE}}/V_{mE}$ and removed the viscosity contribution from $\overline{r_{sm}}$ by using mE results. The $V_{SOD1^{mE}}/V_{mE}$ reaches the highest value at 2 h and then decreases to a level higher than the basal condition at 24 h, indicating that H_2O_2 promotes the SOD1 dimerization.

https://doi.org/10.1021/cbmi.3c00002
Chem. Biomed. Imaging 2023, 1, 49–57

3. CONCLUSION

By introducing a photoconvertible fluorescent protein, mEos4b, and developing the single-molecule fluorescence anisotropy assay, we successfully resolved the antagonistic effects of homo-FRET and molecular rotation on fluorescence anisotropy and applied $\overline{r_{sm}}$ to investigate the in-cell protein responses at the single-molecule level. Using monomeric mEos4b, whose hydrodynamic volume is always constant, allows smFA to investigate the effects of extracellular stimuli on intracellular viscosity. Cytosolic viscosity is correlated with biological functions, such as protein folding[37] and enzyme catalysis.[38] One possible explanation for the observed $\overline{r_{sm}}$ changes of mE is that the cell decreases its intracellular viscosity to enable faster diffusion of antioxidant proteins to mediate stress when encountering high oxidative stresses. After longer treatment, cells reach a new steady state and increase cellular viscosity to slow down antioxidant proteins. The study of H_2O_2-dependent oligomerization of SOD1 provides direct experimental evidence that SOD1 modifies its oligomeric states in cells, which could be a mechanism to strengthen SOD1's usage in scavenging superoxide radicals, mediating H_2O_2-based metabolism signaling, or regulating antioxidant transcriptions.

Although these findings are exciting, several questions, technically or biophysically, need to be addressed. In this study, we have demonstrated that smFA assay is a powerful method to study the relationships between cellular environment changes and protein oligomeric states. However, we can only conclude the changings qualitatively since the $\overline{r_{sm}}$ is incapable of distinguishing different oligomers nor informing the protein oligomeric state changes in real time. Biophysically, to fully explore the oxidant response mechanism of SOD1, several important long-standing questions need to be solved: (i) How do cells spatiotemporally modulate SOD1 oligomerizations in response to environmental changes? (ii) What key redox-sensitive residues induce structural changes leading to different SOD1 oligomeric stoichiometries? One may address these questions by combing super-resolution microscopy, organelle-specific sensor, and non-targeted proteomics[39] to investigate SOD1 behaviors in homozygous knocked-in lines.[40] This will provide physiologically relevant information on where SOD1 modulates its oligomeric state, what local oxidative stress is, and how post-translational modifications may be responsible for the shifts between different SOD1 oligomers.

4. METHODS

4.1. Material Preparations and Characterizations

4.1.1. Construction Preparations of Monomeric mEos4b (mE), Dimeric mEos4b (dmE), and SOD1-mEos4b (SOD1^{mE}). Due to lacking efficient antibodies for mEos4b, a FLAG tag was introduced to commercially available mEos4b to generate a biochemical detectable construct mEos4b-FLAG. The mEos4b-FLAG gene was amplified by PCR from plasmid mEos4b-N1 (a gift from Michael Davidson, Addgene plasmid # 54814; http://n2t.net/addgene:54814; RRID: Addgene_54814) with primer pair BamHI-mEos4b-F and NotI-FLAG-mEos4b-R (containing a FLAG tag, Table S1) using AccuStart II GelTrack PCR SuperMix (QuantaBio 95136-500, annealing temperature, T_a, = 60 °C). The mEos4b in the mEos4b-N1 plasmid was then replaced by PCR-amplified mEos4b-FLAG between cutting sites BamHI (NEB R3136S) and NotI (NEB R3189S) to generate the monomeric mEos4b construct. To generate the dmE construct, we amplified the mEos4b gene by PCR with primer pair EcoRI-mEos4b-F and BamHI-mEos4b-R (Table S1) from plasmid mEos4b-N1 using AccuStart II GelTrack PCR SuperMix (T_a = 60 °C). The amplified mEos4b was then inserted into the monomeric mEos4b plasmid between cutting sites EcoRI (NEB R3101S) and BamHI to generate the dimeric mEos4b construct. The linker sequence between two mEos4b: TTGGATCCACCGGTC-GCCACC. To generate SOD1^{mE}, we PCR amplified the SOD1 gene from template pF151 pcDNA3.1(+)SOD1WT (a gift from Elizabeth Fisher, Addgene plasmid # 26397; http://n2t.net/addgene:26397; RRID: Addgene_26397) with primer pairs XhoI-SOD1-F and BamHI-SOD1-R (Table S1) using AccuStart II GelTrack PCR SuperMix (T_a = 60 °C). The amplified SOD1 gene was then inserted into the monomeric mEos4b plasmid between cutting sites XhoI (NEB 0146) and BamHI to generate the SOD1-mEos4b construct. All constructs were DNA sequence confirmed (Eton Bioscience).

4.1.2. Cell Culture. African green monkey fibroblast COS7 cells (ATCC CRL-1651) were cultured in Dulbecco's modified Eagle medium (DMEM, Gibco 11965) supplied with 10% fetal bovine serum (SAFC 12306C), GlutaMax-I (Gibco 35050), and sodium pyruvate (Gibco 11360) at 37 °C with 5% CO_2. For imaging, red-free DMEM (Gibco 31053) was used instead of DMEM to minimize the fluorescence background contributed by the culture media.

4.1.3. Western Blot of Constructed Plasmids. To confirm the intactness and expression of each fusion protein (mE, dmE, and SOD1^{mE}), we transiently transfected 10^6 COS7 cells with 1 μg of construct DNA using Lipofectamine 2000 (Invitrogen 11668). In short, 100 μL of Opti-MEM medium containing 1 μg of DNA was added into another 100 μL of Opti-MEM medium (Gibco 11058) containing 2 μL of Lipofectamine 2000. The mixture was incubated at room temperature for 5 min and then added to cell dishes. Cells were collected the next day and lysed with 50 mM Tris buffer (pH = 7.4) containing 150 mM NaCl, 1× Triton x-100, 0.1% Sodium dodecyl sulfate, and protease inhibitor (Thermo Scientific 78425). Protein concentrations were measured using BCA assay (Thermo Scientific 23227). Lysates containing the same amount of protein were reduced with 2.5% 2-mercaptoethanol (Sigma-Aldrich M3148) and heated at 98 °C for 10 min. SDS-PAGE was performed using mini-PROTEAN TGX Stain-Free gel (Bio-Rad 4568094) and semi-dry transferred to a PVDF membrane using a Trans-Blot turbo transfer pack (Bio-Rad 1704156). Fusion proteins were detected with anti-FLAG (Rockland 600-401-383, RRID: AB_219374, 1:1000) or anti-SOD1 (Sigma-Aldrich HPA001401, RRID: AB_1080132, 1:5000) antibodies followed by HRP-conjugated anti-rabbit IgG (Jackson ImmonoResearch 115-035-062, 1:10000) and visualized using Western HRP substrate (MilliporeSigma WBKLS0500) under ChemiDoc Imaging System (Bio-Rad 1708370).

4.1.4. Functionality Assay of SOD1^{mE}. The antioxidant activity of fused SOD1^{mE} was tested following previous literature.[41] In short, a Mini-PROTEAN TGX stain-free gel was pre-electrophoresed without SOD1^{mE} in Tris-EDTA buffer (final concentration of Tris, EDTA = 200 mM and 1 mM, respectively; pH = 8.8) at 40 mA at 4 °C for 1 h and left at 4 °C overnight. 10^6 cells were collected in 0.05 M phosphate buffer (pH = 7.8) and sonicated (QSonica model Q125, 20% power for 30 s) on ice. Protein concentrations were measured using BCA assay. 30 μg of total proteins were loaded and resolved in the pre-electrophoresed gel in Tris-glycine buffer (final concentration of Tris, glycine = 25 mM and 200 mM, respectively; pH = 8.3) at 200 V at 4 °C for 2 h. The gel was then incubated in nitro blue tetrazolium (Sigma-Aldrich N5514) phosphate buffer (133.33 μg/mL) in the dark at room temperature for 45 min. After rinsing with deionized water, the gel was immersed in a riboflavin-TEMED-phosphate buffer (riboflavin (Sigma-Aldrich R7649)/phosphate buffer: 10 μg/mL, TEMED (Bio-Rad 161-0800)/phosphate buffer concentration: 2 μg/50 mL) in the dark for 15 min before exposed to ambient light. Once bands showed up, the gel was imaged using the Chemidoc imaging system.

4.2. Single-Molecule Fluorescence Anisotropy Imaging

4.2.1. Imaging Sample Preparation. A homemade glass chamber (#1.5 coverslip, Globe Scientific #1404-15) was coated with poly-L-lysine buffer (poly-L-lysine (Sigma P1399) with a final concentration of 0.1 mg/mL in 50 mM borate buffer) overnight for

https://doi.org/10.1021/cbmi.3c00002
Chem. Biomed. Imaging 2023, 1, 49−57

cell-immobilization purpose. Coated chambers were washed via phosphate-buffered saline (PBS, Corning 21-031-CM) 3 times and dried out. COS7 cells were seeded on the coated chambers and cultured in a red-free complete DMEM medium for 1 day before transfection. The constructs were introduced into cells using Lipofectamine 2000. After transfection, cells were further incubated at 37 °C to allow transfected protein production for one extra day. On the imaging day, the culture media of COS7 cells were refreshed with red-free complete DMEM (i.e., basal condition) or DMEM with 100 μM of H_2O_2 (Sigma-Aldrich 654833) for 2 h (i.e., H_2O_2, 2 h condition) or 24 h (i.e., H_2O_2, 24 h condition) before mounting chambers on the microscope.

4.2.2. Microscope Setup. All single-molecule fluorescence anisotropy images were obtained via a home-built microscope system (Figure 1B) that is equipped with an inverted microscope (Olympus IX83), a high numerical aperture objective (Olympus, UAPON 100×, NA = 1.49), and a CMOS camera (Photometric Prime 95B). To capture single-molecule signals in live COS7 cells, we use a low-power 405 nm laser (Coherent S160528012, ∼0.2 W/cm^2 for 10 ms) to photoconvert mEos4b from green into red fluorescent proteins sparsely. The photoconverted red mEos4b was excited with a continuous wave (cw) 552 nm laser (Coherent SKU 1284009, ∼30 kW/cm^2 for 3 ms). The red fluoresce of mEos4b was collected by the objective and captured by the camera with a 3 ms integration time for 30 frames before another photoconversion excitation. To obtain robust fluorescence anisotropy readouts, we performed all imaging at 25 °C, which helps slow down the molecular rotational and diffusional movement during image acquisition.

In the excitation path, the coaxial 405 and 552 nm lasers enter from the backport of the microscope, get reflected by a dichroic mirror (Chroma ET-391-32/479-33/554-24/638-31 Multi LED set, Chroma 89402), enter the objective, and activate or excite the mEos4b. A combination of the half-wave plate (Thorlabs WPH10M-405 for 405 nm laser and WPH10M-561 for 552 nm laser) and the polarizer (Thorlabs GL10-A) was used to control laser intensity and ensure the laser excites the mEos4b with a parallel polarization. The beam diameter at the focus plane is ∼11 μm. In the detection path, emission from excited mEos4b was collected by the objective and passed through a dichroic mirror and a band-pass filter (Chroma ET610/60 nm). Filtered emissions entered a polarization beam splitter (Thorlabs PBS201) to separate the parallel and perpendicular polarization components, which were later sent to a CMOS camera for two-channel imaging.

4.2.3. $\overline{r_{sm}}$ and $\overline{r_{cell}}$ Quantification. After localizing single-molecule spots in Im_{com} using a home-built MATLAB program, spots showing higher spot intensity/amplitude and higher noise than that in the COS7 cell-only control were further selected for subsequent analyses (Figure S2). The fluorescence intensities of these spots from the parallelly ($I_\parallel$) and perpendicularly ($I_\perp$) polarized channels were calculated by integrating the pixel counts of a 3-by-3 area (centered at the spot location) to quantify $I_\parallel$ and $I_\perp$. The fluorescence anisotropy of a single molecule was then calculated via $r_{sm} = \frac{I_\parallel - I_\perp}{I_\parallel + 2\cdot I_\perp}$. Averaging of all single-molecule fluorescence anisotropy gives the mean ($\overline{r_{sm}}$). Similar analyses were conducted at the single-cell level. For each cell, r_{cell} was calculated by averaging all r_{sm}. The mean of the cellular fluorescence anisotropy ($\overline{r_{cell}}$) was calculated by averaging the r_{cell} of all cells. All error bars represent the standard error of the mean.

4.3. Ensemble Fluorescence Anisotropy Quantification

In contrast to the single-molecule fluorescence anisotropy measurements probing the anisotropy of red fluorescence of photoconverted mEos4b, ensemble fluorescence anisotropy estimates the anisotropy of the green fluorescence of mEos4b. By replacing the 552 nm in the home-built microscope system, we excite the green mEos4b with a cw 488 nm laser (Coherent S16062206, ∼187 mW/cm^2 for 20 ms). The green fluorescence passed a band-pass filter (Chroma ET525/52 nm) and the beam splitter and finally arrived CMOS camera for two-channel imaging. All imaging experiments were conducted at 25 °C to ensure a proper comparison between single-molecule and ensemble fluorescence anisotropy measurements. To estimate the ensemble fluorescence anisotropy, r_{ens}, we collected 5000 images and analyzed the green fluorescence intensity of cytosolic regions. The same experiments were performed with COS7 cells to estimate the cellular background contributions. After background subtraction, intensities of the cytosolic regions in parallelly polarized and perpendicularly polarized channels were averaged to generate the $F_\parallel$ and $F_\perp$, respectively. The final ensemble fluorescence anisotropy was calculated through $r_{ens} = \frac{F_\parallel - F_\perp}{F_\parallel + 2\cdot F_\perp}$. The mean of the ensemble fluorescence anisotropy ($\overline{r_{ens}}$) was calculated by averaging the r_{ens} of all cells. All error bars represent the standard error of the mean.

■ ASSOCIATED CONTENT

Supporting Information

The Supporting Information is available free of charge at https://pubs.acs.org/doi/10.1021/cbmi.3c00002.

Western blot results of all constructs, estimation of background contributions to single-molecule signals, and primers used for plasmids (PDF)

■ AUTHOR INFORMATION

Corresponding Author

Tai-Yen Chen − *Department of Chemistry, University of Houston, Houston, Texas 77204, United States;* orcid.org/0000-0002-2881-3068; Email: tchen37@central.uh.edu

Author

Huanhuan Chen − *Department of Chemistry, University of Houston, Houston, Texas 77204, United States*

Complete contact information is available at: https://pubs.acs.org/10.1021/cbmi.3c00002

Author Contributions

H.C. operated the experiments and analyzed the data. All authors were involved in interpreting data and paper preparation.

Notes

The authors declare no competing financial interest.

■ ACKNOWLEDGMENTS

This work was supported by the National Institutes of Health (Grant No. R35GM133505) and the University of Houston.

■ REFERENCES

(1) Fernandez-Fernandez, S.; Almeida, A.; Bolaños, J. P. Antioxidant and bioenergetic coupling between neurons and astrocytes. *Biochemical Journal* **2012**, *443* (1), 3−11.

(2) Bélanger, M.; Allaman, I.; Magistretti, P. J. Brain energy metabolism: focus on astrocyte-neuron metabolic cooperation. *Cell Metabolism* **2011**, *14* (6), 724−738.

(3) Poyton, R. O.; Ball, K. A.; Castello, P. R. Mitochondrial generation of free radicals and hypoxic signaling. *Trends in Endocrinology & Metabolism* **2009**, *20* (7), 332−340.

(4) St-Pierre, J.; Buckingham, J. A.; Roebuck, S. J.; Brand, M. D. Topology of superoxide production from different sites in the mitochondrial electron transport chain. *J. Biol. Chem.* **2002**, *277* (47), 44784−44790.

(5) Sun, J.; Trumpower, B. L. Superoxide anion generation by the cytochrome bc1 complex. *Archives of Biochemistry and Biophysics* **2003**, *419* (2), 198−206.

(6) Hongpaisan, J.; Winters, C. A.; Andrews, S. B. Calcium-dependent mitochondrial superoxide modulates nuclear CREB phosphorylation in hippocampal neurons. *Molecular and Cellular Neuroscience* **2003**, *24* (4), 1103−1115.
(7) Brennan, A. M; Won Suh, S.; Joon Won, S.; Narasimhan, P.; Kauppinen, T. M; Lee, H.; Edling, Y.; Chan, P. H; Swanson, R. A NADPH oxidase is the primary source of superoxide induced by NMDA receptor activation. *Nature Neuroscience* **2009**, *12* (7), 857−863.
(8) Milani, P.; Ambrosi, G.; Gammoh, O.; Blandini, F.; Cereda, C. SOD1 and DJ-1 Converge at Nrf2 Pathway: A Clue for Antioxidant Therapeutic Potential in Neurodegeneration. *Oxidative Medicine and Cellular Longevity* **2013**, *2013*, 836760.
(9) Baxter, P. S.; Hardingham, G. E. Adaptive regulation of the brain's antioxidant defences by neurons and astrocytes. *Free Radical Biology and Medicine* **2016**, *100*, 147−152.
(10) García-Caparrós, P.; De Filippis, L.; Gul, A.; Hasanuzzaman, M.; Ozturk, M.; Altay, V.; Lao, M. T. Oxidative Stress and Antioxidant Metabolism under Adverse Environmental Conditions: a Review. *Botanical Review* **2021**, *87*, 421.
(11) Lee, K. H.; Cha, M.; Lee, B. H. Neuroprotective Effect of Antioxidants in the Brain. *International Journal of Molecular Sciences* **2020**, *21* (19), 7152.
(12) Trist, B. G.; Hilton, J. B.; Hare, D. J.; Crouch, P. J.; Double, K. L. Superoxide Dismutase 1 in Health and Disease: How a Frontline Antioxidant Becomes Neurotoxic. *Angew. Chem., Int. Ed.* **2021**, *60* (17), 9215−9246.
(13) Culik, R. M.; Sekhar, A.; Nagesh, J.; Deol, H.; Rumfeldt, J. A. O.; Meiering, E. M.; Kay, L. E. Effects of maturation on the conformational free-energy landscape of SOD1. *Proc. Natl. Acad. Sci. U. S. A.* **2018**, *115* (11), No. E2546-E2555.
(14) Sekhar, A.; Rumfeldt, J. A. O.; Broom, H. R.; Doyle, C. M.; Bouvignies, G.; Meiering, E. M.; Kay, L. E. Thermal fluctuations of immature SOD1 lead to separate folding and misfolding pathways. *eLife* **2015**, *4*, No. e07296.
(15) Arnesano, F.; Banci, L.; Bertini, I.; Martinelli, M.; Furukawa, Y.; O'Halloran, T. V. The unusually stable quaternary structure of human Cu, Zn-superoxide dismutase 1 is controlled by both metal occupancy and disulfide status. *J. Biol. Chem.* **2004**, *279* (46), 47998−48003.
(16) Proctor, E. A.; Fee, L.; Tao, Y.; Redler, R. L.; Fay, J. M.; Zhang, Y.; Lv, Z.; Mercer, I. P.; Deshmukh, M.; Lyubchenko, Y. L.; Dokholyan, N. V. Nonnative SOD1 trimer is toxic to motor neurons in a model of amyotrophic lateral sclerosis. *Proc. Natl. Acad. Sci. U. S. A.* **2016**, *113* (3), 614−619.
(17) Zhu, C.; Beck, M. V.; Griffith, J. D.; Deshmukh, M.; Dokholyan, N. V. Large SOD1 aggregates, unlike trimeric SOD1, do not impact cell viability in a model of amyotrophic lateral sclerosis. *Proc. Natl. Acad. Sci. U. S. A.* **2018**, *115* (18), 4661−4665.
(18) Squire, A.; Verveer, P. J.; Rocks, O.; Bastiaens, P. I. H. Red-edge anisotropy microscopy enables dynamic imaging of homo-FRET between green fluorescent proteins in cells. *J. Struct. Biol.* **2004**, *147* (1), 62−69.
(19) Gautier, I.; Tramier, M.; Durieux, C.; Coppey, J.; Pansu, R.; Nicolas, J.-C.; Kemnitz, K.; Coppey-Moisan, M. Homo-FRET microscopy in living cells to measure monomer-dimer transition of GFP-tagged proteins. *Biophysical Journal* **2001**, *80* (6), 3000−3008.
(20) Bader, A. N.; Hofman, E. G.; Voortman, J.; van Bergen en Henegouwen, P. M. P.; Gerritsen, H. C. Homo-FRET imaging enables quantification of protein cluster sizes with subcellular resolution. *Biophysical Journal* **2009**, *97* (9), 2613−2622.
(21) Heckmeier, P. J.; Agam, G.; Teese, M. G.; Hoyer, M.; Stehle, R.; Lamb, D. C.; Langosch, D. Determining the stoichiometry of small protein oligomers using steady-state fluorescence anisotropy. *Biophysical Journal* **2020**, *119* (1), 99−114.
(22) Jameson, D. M.; Seifried, S. E. Quantification of protein-protein interactions using fluorescence polarization. *Methods* **1999**, *19* (2), 222−233.
(23) Haque, M. E.; Spremulli, L. L.; Fecko, C. J. Identification of protein-protein and protein-ribosome interacting regions of the C-terminal tail of human mitochondrial inner membrane protein Oxa1L. *J. Biol. Chem.* **2010**, *285* (45), 34991−34998.
(24) Ojha, N.; Rainey, K. H.; Patterson, G. H. Imaging of fluorescence anisotropy during photoswitching provides a simple readout for protein self-association. *Nat. Commun.* **2020**, *11* (1), 21.
(25) Rainey, K. H.; Patterson, G. H. Photoswitching FRET to monitor protein-protein interactions. *Proc. Natl. Acad. Sci. U. S. A.* **2019**, *116* (3), 864−873.
(26) Misiura, A.; Dutta, C.; Leung, W.; Zepeda O, J.; Terlier, T.; Landes, C. F. The competing influence of surface roughness, hydrophobicity, and electrostatics on protein dynamics on a self-assembled monolayer. *J. Chem. Phys.* **2022**, *156* (9), 094707.
(27) Chen, H.; Xie, X.; Chen, T.-Y. Single-molecule microscopy for in-cell quantification of protein oligomeric stoichiometry. *Curr. Opin. Struct. Biol.* **2021**, *66*, 112−118.
(28) Xie, X.; Cheng, Y.-S.; Wen, M.-H.; Calindi, A.; Yang, K.; Chiu, C.-W.; Chen, T.-Y. Quantifying the Oligomeric States of Membrane Proteins in Cells through Super-resolution Localizations. *J. Phys. Chem. B* **2018**, *122* (46), 10496−10504.
(29) Santiago, A. G.; Chen, T.-Y.; Genova, L. A.; Jung, W.; George Thompson, A. M.; McEvoy, M. M.; Chen, P. Adaptor protein mediates dynamic pump assembly for bacterial metal efflux. *Proc. Natl. Acad. Sci. U. S. A.* **2017**, *114* (26), 6694−6699.
(30) Martell, D. J.; Joshi, C. P.; Gaballa, A.; Santiago, A. G.; Chen, T.-Y.; Jung, W.; Helmann, J. D.; Chen, P. Metalloregulator CueR biases RNA polymerase's kinetic sampling of dead-end or open complex to repress or activate transcription. *Proc. Natl. Acad. Sci. U. S. A.* **2015**, *112* (44), 13467−13472.
(31) Chen, T.-Y.; Santiago, A. G.; Jung, W.; Krzeminski, Łu.; Yang, F.; Martell, D. J.; Helmann, J. D.; Chen, P. Concentration-and chromosome-organization-dependent regulator unbinding from DNA for transcription regulation in living cells. *Nat. Commun.* **2015**, *6*, 7445.
(32) Paez-Segala, M. G; Sun, M. G; Shtengel, G.; Viswanathan, S.; Baird, M. A; Macklin, J. J; Patel, R.; Allen, J. R; Howe, E. S; Piszczek, G.; Hess, H. F; Davidson, M. W; Wang, Y.; Looger, L. L Fixation-resistant photoactivatable fluorescent proteins for CLEM. *Nat. Methods* **2015**, *12* (3), 215−218.
(33) Albrecht, C.; Joseph, R. *Lakowicz: Principles of Fluorescence Spectroscopy*; Springer, 2008.
(34) Jameson, D. M.; Ross, J. A. Fluorescence polarization/anisotropy in diagnostics and imaging. *Chem. Rev.* **2010**, *110* (5), 2685−2708.
(35) Kubánková, M.; Summers, P. A.; Löpez-Duarte, I.; Kiryushko, D.; Kuimova, M. K. Microscopic viscosity of neuronal plasma membranes measured using fluorescent molecular rotors: Effects of oxidative stress and neuroprotection. *ACS Appl. Mater. Interfaces* **2019**, *11* (40), 36307−36315.
(36) Heo, S.; Kim, S.; Kang, D. The role of hydrogen peroxide and peroxiredoxins throughout the cell cycle. *Antioxidants* **2020**, *9* (4), 280.
(37) Klimov, D.; Thirumalai, D. Viscosity dependence of the folding rates of proteins. *Physical Review Letters* **1997**, *79* (2), 317.
(38) Blacklow, S. C.; Raines, R. T.; Lim, W. A.; Zamore, P. D.; Knowles, J. R. Triosephosphate isomerase catalysis is diffusion controlled. *Biochemistry* **1988**, *27* (4), 1158−1165.
(39) Zhang, Y.; Wen, M.-H.; Qin, G.; Cai, C.; Chen, T.-Y. Subcellular redox responses reveal different Cu-dependent antioxidant defenses between mitochondria and cytosol. *Metallomics* **2022**, *14* (11), mfac087.
(40) Huang, P.-S.; Wen, M.-H.; Xie, X.; Xu, A.; Lee, D.-F.; Chen, T.-Y. Generation of a homozygous knock-in human embryonic stem cell line expressing SNAP-tagged SOD1. *Stem Cell Research* **2021**, *54*, 102415.
(41) Weydert, C. J.; Cullen, J. J. Measurement of superoxide dismutase, catalase and glutathione peroxidase in cultured cells and tissue. *Nat. Protoc.* **2010**, *5* (1), 51−66.

https://doi.org/10.1021/cbmi.3c00002
Chem. Biomed. Imaging 2023, 1, 49−57